Localization of Mars rovers using descent and surface-based image data

Rongxing Li, Fei Ma, and Fengliang Xu

Department of Civil and Environmental Engineering and Geodetic Science, Ohio State University, Columbus, Ohio, USA

Larry H. Matthies and Clark F. Olson

Jet Propulsion Laboratory, California Institute of Technology, Pasadena, California, USA

Raymond E. Arvidson

Department of Earth and Planetary Sciences, Washington University, St. Louis, Missouri, USA

[1]   The planned 2003 Mars Exploration Rover (MER) Mission and follow-on surface activities associated with landed missions will focus on long distance roving and sample return, which require detailed knowledge of vehicle locations in both local and global reference systems. In this paper we argue that this rover localization should be known to within 0.1 of the distance traversed for local coordinate systems. To test the ability to meet this goal using only descent and rover-based data, we conducted experiments with simulated descent images and Field Integrated Design and Operations Rover data collected during field tests at Silver Lake, California, in April 1999. Specifically, an integrated bundle adjustment system incorporating both descent and rover-based images was developed and used to localize the rover positions. On the basis of surveyed ground control points it is demonstrated that the joint analysis produces RMS errors of 0.24, 0.15, and 0.38 m in x, y, and z% directions in a local coordinate system, respectively, for ground points within 500 m from the landing point and 0.23, 0.21, and 0.46 m within a distance of 1.5 km. Results show that it is possible to meet the 0.1 goal using descent and rover-based data only.   *INDEX TERMS:* 1224 Geodesy and Gravity: Photogrammetry; 5464 Planetology: Solid Surface Planets: Remote sensing; 5494 Planetology: Solid Surface Planets: Instruments and techniques; 6225 Planetology: Solar System Objects: Mars; *KEYWORDS:* Mars rover, localization, mapping, topography, bundle adjustment, navigation

1. Introduction

[2]   The purpose of this paper is to explore and test a method of locating Mars rovers within local coordinate systems using a combined reduction of descent and rover-based image data. The Mars Pathfinder Mission in 1997 clearly demonstrated the importance of mobility systems in that the Sojourner Rover provided powerful close-range exploration tools for microscale rock investigation, soil research, and other scientific objectives within an area of ~10 m × 10 m from the lander [*Raeburn and Golombek*, 1998; *Golombek et al.*, 1997]. In the planned 2003 Mars Exploration Rover (MER) Mission two rovers will be on the surface, each traversing up to 1 km, acquiring remote sensing and in situ data as they travel across the surface. Unfortunately, neither Pathfinder nor MER have the advantage of descent image data to help localize rover positions within a local coordinate system. For Pathfinder the use of the Imager for Mars Pathfinder (IMP) cameras on the lander mitigated the lack of descent data. For MER the lack of sufficient descent images will present challenges associated with determining rover locations within existing orbital image data with a few meters spatial resolution, i.e., Mars Orbital Camera (MOC). In the future, (HRSC) high-resolution stereo camera and super resolution camera (SRC) imaging systems may supply stereo images of resolutions of 10 and 2.3 m, respectively, for a landing site [*Albertz et al.*, 1996; *Pischel et al.*, 2001]. The Mars Reconnaissance Orbiter will obtain images of a resolution better than 0.5 m. However, Mars descent images have hierarchical resolutions and the vertical stereo imaging capability. They can be used for bridging orbital and ground images and have unmatchable potential for supporting local landing site characterization. In this paper we demonstrate the ability to locate rover positions to within 0.1% accuracy and further that descent image data are important to reach this accuracy.

[3]   Specifically, we present the results of rover localization experiments using descent and rover image data acquired at the field test site at Silver Lake, California [*Li et al.*, 2000]. Different bundle adjustment models have been used to localize the rover, in which ground control points, tie points, camera calibration parameters, and various distortion parameters were taken into account. Using the new bundle adjustment system, we are able to integrate the

descent and rover images to achieve RMS errors of 0.24, 0.15, and 0.38 m in the x, y, and z directions in a local coordinate system, respectively, for a distance of up to 500, 0.23, 0.21, and 0.46 m within 1.5 km. The results demonstrate the potential of the introduced method for the goal of a rover localization accuracy of up to 0.1%.

2. Background Discussion

[4] The rover localization accuracy is a critical factor that affects a number of design and operation issues. On the basis of our analysis of the simulation data collected at Silver Lake, California, we can achieve a localization accuracy of 0.1% of the traversed distance. Such a high accuracy is important for rover navigation purposes. Since rover lifetime will be limited it is necessary to maximize its ability to accurately move from point to point according to the designed operation plan. It will also include returning to the landing site to deliver samples, and traversing back to the same place to collect the same samples again if needed. Suppose that we could see a fresh looking crater of the minimal size in a descent image and wanted to have the rover get there from the maximum distance across the descent image. Taking 10 m as the crater diameter and 10 km as the diameter of the descent image, the distance from the descent center to the crater traversed by the rover, the rover localization accuracy should be 10 m/10 km, namely, 0.1% of the distance traversed. On the other hand, if the descent image size is ∼1000 pixel × 1000 pixel, 0.1% of the image size is one pixel. Therefore we set the 0.1% localization accuracy as our goal. However, in reality, to expect many unforeseeable influencing factors, a localization accuracy of 0.4% may be tolerable. This accuracy corresponds to a 20-m crater at a traversing distance of 5 km.

[5] Research has been carried out on rover localization using several different methods. *Volpe et al.* [1995] developed a method that uses images of a colored cylindrical target to estimate position and heading information for the rover. The distance from the rover to the target is derived from the measured size and centroid disparity of the cylinder, and the angle is determined by analyzing the visible color quadrants and the degree of visibility. Within a 10-m range the achieved accuracy is typically 5° for heading and 5% for distance. Another approach tested maximum likelihood estimation techniques for performing rover self-localization in natural terrain by matching range maps [*Olson and Matthies*, 1998]. This technique can find the best position and does not require an initial estimate of the rover position. This paper discusses large-scale surface mapping and rover localization using descent and rover images based on photogrammetric methods to achieve a much higher localization accuracy.

[6] The descent images taken from ∼5000 m to several meters above the ground have a hierarchy of resolutions (from coarse to fine), which match those of the orbital images and the ground lander and rover images. This makes descent images extremely valuable to scientists for mission planning and to engineers for operating the rover. Specifically, for rover localization the descent images provides an effective way to enhance the geometry by integrating orbital, descent and lander/rover images to form an image network. In general, a traditional aerial triangulation for earth mapping purposes is performed on pairs or strips of images at nearly the same altitude (horizontal baselines) and with large areas of overlapping. In contrast, we are dealing with descent images that have vertical baselines. The overlapping area decreases as the altitude decreases and the image resolution increases. Photogrammetric triangulations using the combined data set of descent and rover images face challenges of special geometry, multiple resolution, and the same ground features sensed from two perpendicular directions.

3. Photogrammetric Modeling for Descent Images

3.1. Potential of the Descent Images

[7] Conventional aerial earth photographs are usually taken at nearly the same altitude with a regular overlapping area of ∼60%. However, the descent images are acquired at a sequence of decreasing altitudes. Landmarks may appear in multiple descent images with different resolutions, with the degree of detail decreasing as the image resolution decreases. Because of the resolution variance in the image sequence, it is very difficult to find ground features that appear in all the descent images and are appropriate for selection as tie points to form an image network. Therefore the tie points may be chosen as those appearing in a few adjacent images whose resolution differences are not significant. Thus the resulting tie points link the descent image sequence hierarchically in the vertical direction.

[8] In an ideal situation a descent image can be treated as vertical photography [*Wolf*, 1983], and the rotation matrix can be simplified to

$$\begin{pmatrix} m_{11} & m_{12} & m_{13} \\ m_{21} & m_{22} & m_{23} \\ m_{31} & m_{32} & m_{33} \end{pmatrix} = \begin{pmatrix} \cos\kappa & \sin\kappa & 0 \\ -\sin\kappa & \cos\kappa & 0 \\ 0 & 0 & 1 \end{pmatrix}, \quad (1)$$

where κ is the rotation angle about the z axis. The collinearity equations are then

$$x_p = -f \frac{m_{11}(X_P - X_0) + m_{12}(Y_P - Y_0)}{m_{33}(Z_P - Z_0)},$$

$$y_p = -f \frac{m_{21}(X_P - X_0) + m_{22}(Y_P - Y_0)}{m_{33}(Z_P - Z_0)} \quad (2)$$

with (X_0, Y_0, Z_0) being the exposure center position, (X_P, Y_P, Z_P) the object point position, F focal length, and (x_p, y_p) the measured image point. If we measure corresponding image points in any two stereo descent images, we will be able to determine the location of the corresponding three-dimensional (3-D) object. Suppose the vertical descent image orientation parameters are fixed, the linearized collinearity equations are

$$dx_p = -\frac{f\cos\kappa}{Z_P - Z_0} dX_P - \frac{f\sin\kappa}{Z_P - Z_0} dY_P - \frac{x_p}{Z_P - Z_0} dZ_P$$

$$dy_p = \frac{f\sin\kappa}{Z_P - Z_0} dX_P - \frac{f\cos\kappa}{Z_P - Z_0} dY_P - \frac{y_p}{Z_P - Z_0} dZ_P. \quad (3)$$
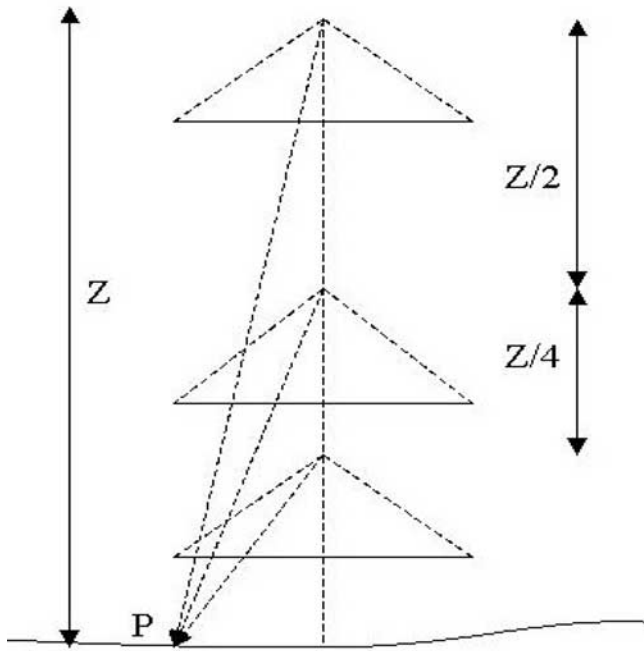
Figure 1. Geometry of the descent images.

Therefore the lower resolution at the higher imaging altitude Z_0 results in a greater contribution of image measurement errors to the uncertainties in the 3-D ground coordinates (equation (3)).

[9] Figure 1 illustrates the geometry of the descent images. In principle, if any two consecutive descent images are strictly on the same vertical line, there is no parallax at the center of the images. However, slight deviations of the individual images from the center create parallaxes between adjacent pairs (Figure 2). Away from the center, the parallax increases. If there are sufficient ground features in the overlapping area, there should be enough tie points selected from the images to determine the image orientation parameters. For the entire descent image sequence a bundle adjustment algorithm should be able to handle the tie points that are hierarchically distributed in the consecutive images and estimate the optimal image orientation parameters [*Li et*

al., 2000]. The 3-D ground coordinates of the tie points can be computed after the bundle adjustment.

3.2. Bundle Adjustment of a Free Descent Image Network

[10] In the environment of a Mars landing site, there will be no ground control. The landing site error ellipse determined through radio tracking is about hundreds of kilometers. A UHF radio link between the orbiter and the rover may supply the rover position at an accuracy of ∼100 m within a few days after landing. This absolute location can be combined with an azimuth pointing to a landmark defined in the latest global Mars control network with a point accuracy of 750 m [*Zeitler et al.*, 2000]. The absolute accuracy of the landmark may be improved in the future when the global Mars control network is enhanced by the integrated MOC, MOLA, and HRSC data. The image network in the bundle adjustment computation is then a "free" network consisting of exposure centers of the descending camera positions, measured image tie points, and their corresponding ground points, without any ground control points. In the adjustment model we define a local coordinate system where the origin is the landing center. After landing this center can be determined by the radio link or matching the descent image sequence with high-resolution orbital data such as MOC and HRSC images. Similarly, another distinguished landmark, preferably a landmark that is in the global Mars control network and farther away from the landing center, can be selected. The two landmarks selected in this way may not have a high absolute accuracy in the global coordinate system. However, it provides a link between the data collected at the local landing site and the global Mars exploration data. It will not affect the relative accuracy and the operations within the local coordinate system. Another way to establish the link is to have the same landing center and use the remote landmark just for providing the azimuth angle. The scale information comes from the camera base, the distance between the two stereo cameras that can be calibrated before launching.

[11] The above link between the landing site and the global coordinate system can be implemented as three constraints, namely, a scale, an azimuth, and a zenith. Suppose (X_0, Y_0, Z_0) are coordinates of the landing center, they become $(0, 0, 0)$ in the local coordinate system.
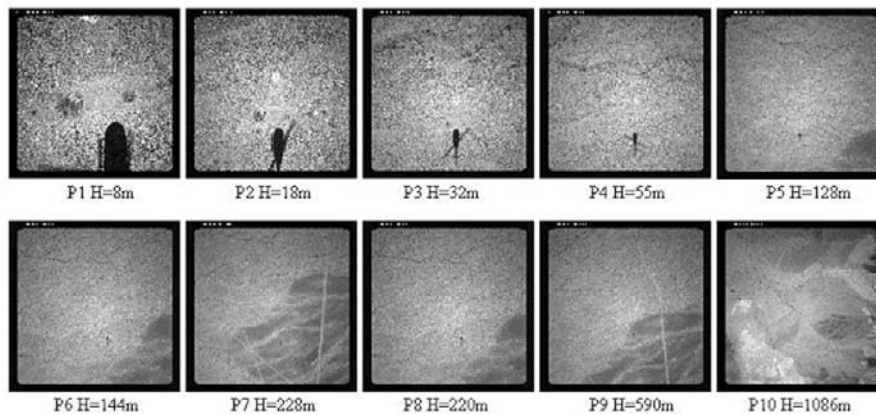

Figure 2. A set of simulated descent images.

Further, (X_E, Y_E, Z_E) are coordinates of the recognized landmark. Given the distance between the two points as S, the scale constraint is

$$(X_E - X_0)^2 + (Y_E - Y_0)^2 + (Z_E - Z_0)^2 = S^2. \tag{4}$$

[12] Subsequently, assume that the azimuth and zenith angles of the landmark with respect to the landing center are α and β. The azimuth and zenith constraints can be expressed as

$$\alpha = \tan^{-1} \frac{Y_E - Y_0}{X_E - X_0},$$

$$\beta = \tan^{-1} \frac{Z_E - Z_0}{\sqrt{(X_E - X_0)^2 + (Y_E - Y_0)^2}}. \tag{5}$$

[13] If P denotes the weight matrix of the measurements of image points, we have the observation equation

$$V = AX - L, \tag{6}$$

where V is the correction vector, A the coefficient matrix after linearization, x the unknown vector including the orientation parameters of the images and ground coordinates of the tie points, and L the observation vector. The three constraints can be represented as

$$HX = W. \tag{7}$$

The network can be solved by an extended least squares adjustment in that we apply the least squares principle

$$\sum_{i=1}^{m} v_i^2 = \min \tag{8}$$

with the additional requirement

$$\sum_{i=1}^{n} x_i^2 = \min. \tag{9}$$

[14] In computation the normal matrix N is defined as $A^T P A$ and is decomposed into matrices U and V, and a diagonal matrix D: $N = A^T P A = U D V^T$. If the rank of N is I and d_i is the diagonal elements of D, $d_i > 0$ and $1 \leq i \leq I$, the generalized inverse of N is calculated as

$$N^- = V \cdot \left[diag\left(\frac{1}{d_j}\right) \right] \cdot U^T. \tag{10}$$

Finally, the solution becomes

$$X = N^- \left\{ (A^T PL) + H^T (HN^- H^T)^{-1} [W - HN^- (A^T PL)] \right\}. \tag{11}$$

The unit weight variance is

$$\sigma_0^2 = \frac{\sum_{i=1}^{m} r_i^2}{m - \text{rank}(N)}. \tag{12}$$

Here m is the number of observations in (6). The covariance matrix of the unknown vector X is

$$\Sigma_x = \sigma_0^2 \left[N^- - N^- H^T (HN^- H^T)^{-1} HN^- \right]. \tag{13}$$

4. Rover Localization Using Descent and Rover Images

[15] The above model can also be used to integrate the rover images with the descent images, so that the rover locations are included in the rover camera orientation parameters that are estimated within the bundle adjustment computation. Tie points between the rover and descent images must be selected to facilitate the integration. A more efficient way to perform the computation and to implement it in an autonomous environment with limited computational capacity is the so-called incremental bundle adjustment. Assume that we have processed observations from the descent images and first m-1 rover stations. Now we measure tie points between the descent images and rover images of the m-1 rover stations, as well as those between the descent images and the current rover station (m). The observation equation of (6) is decomposed into two parts

$$v_{m-1} = A_{m-1} X_{m-1} - l_{m-1}, \tag{14}$$

$$v_m = A_m X_m + B_m Y_m - l_m. \tag{15}$$

[16] Equation (14) represents the relationship between the observations upto rover station m-1 and unknowns X, including rover positions up to station m-1. The new rover position of rover station m is contained in the new unknown vector y in (15). Suppose the generalized inverse of the normal matrix of (14) and (15) is

$$N_m^- = \begin{pmatrix} A_{m-1}^T P_{m-1} A_{m-1} + A_m^T P_m A_m & A_m^T P_m B_m \\ B_m^T P_m A_m & B_m^T P_m B_m \end{pmatrix}^- = \begin{pmatrix} K_m & G_m \\ G_m^T & H_m \end{pmatrix},$$

then the solution using all the observations up to station m is

$$\begin{pmatrix} X_m \\ Y_m \end{pmatrix} = \\ \begin{pmatrix} \bar{W}_m [X_{m-1} - F_m(l_m - A_m X_{m-1})] + G_m B_m^T P_m l_m \\ -(B_m^T P_m B_m)^- B_m^T P_m A_m \bar{W}_m [X_{m-1} - F_m(l_m - A_m X_{m-1})] + H_m B_m^T P_m l_m \end{pmatrix}. \tag{16}$$
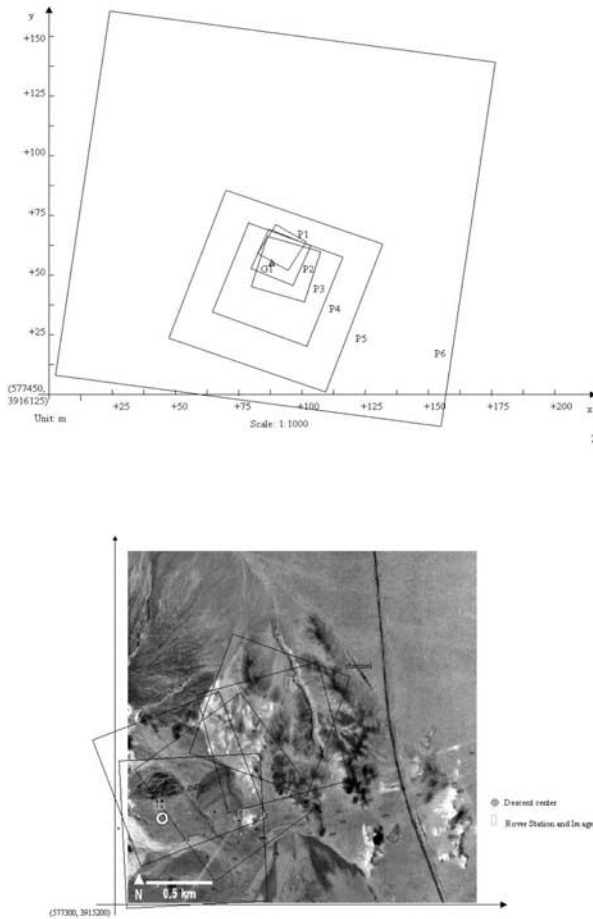
The covariance matrix is expressed by

$$\sum_m \begin{pmatrix} X_m \\ Y_m \end{pmatrix} = N_m^- N_m N_m^-, \tag{17}$$

where

$$N_m^- = (N_{m-1} + A_m^T P_m A_m)^- \\ = (A_{m-1}^T P_{m-1} A_{m-1})^- - F_m A_m (A_{m-1}^T P_{m-1} A_{m-1})^-,$$

$$\bar{W}_m = I + \bar{N}_m^- A_m^T P_m B_m H_m B_m^T P_m A_m^T,$$

$$F_m = (A_{m-1}^T P_{m-1} A_m)^- A_m^T [P_m^{-1} + A_m (A_{m-1}^T P_{m-1} A_{m-1})^- A_m^T]^{-1}.$$

Figure 3. Footprints of descent images: (a) six lower descent images (P1 to P6, also see Figure 2) and a ground control point (G1), and (b) five additional descent images ∼1.5 km from the descending center.

[17] In (15), in order to estimate the new rover positions in Y_m we will only deal with coefficient matrices computed using the new observations and the part of the network that is linked to the new rover stations. This can reduce the computational intensity and can be used for on-board computation for rover localization. The previous rover positions in X_m will also be updated in (15).

5. Experimental Results

### 5.1. Acquisition of Simulated Descent Images and Rover Images

[18] A descent imaging system was successfully used for lunar exploration (NASA, 2001:http://cass.jsc.nasa.gov/expmoon/Apollo11/A11_Photography.html). A descent camera, Mars Descent Imager (MARDI), manufactured by Malin Space Science Systems (MSSS), was mounted on the Mars spacecraft of the failed Mars Polar Lander Mission in 1999 (MSSS, 2001:http://www.msss.com; OSU-MGL, 2001:http://shoreline.eng.ohio-state.edu/research/mars/mardi.htm). MARDI has a focal length of 7.135 mm, a field of view (FOV) of 73.4° and an image size 1024 × 1024 pixels. The descent images used in this experiment were acquired using a helicopter-borne imag-

ing system that simulated the descending process of a spacecraft.

[19] Following the Field Integrated Design and Operations (FIDO) rover test in 20–29 April 1999, at Silver Lake, California [*Arvidson et al.*, 2002], an experiment of descent imaging simulation was carried out using a helicopter-borne imaging system consisting of differential GPS receivers, an inertial navigation system (INS), and a digital camera. Manufactured by Lockheed Martin Fairchild Semiconductors, the CCD chip has 4096 × 4096 pixels and an imaging area of 60 mm by 60 mm (15-micron pixel size). The camera has a focal length of 51.7 mm and a FOV of 62°. The resolution difference between MARDI and this camera should not affect the result significantly because the descent image series of both cameras are capable of providing an image network that has hierarchical resolutions from the ground to the high altitude. The measurements from the hierarchical images should be able to supply a similar quality of tie points for the bundle adjustment computation and reach compatible results.

[20] Fifteen descent images were taken from a helicopter that simulated the descent process and allowed imaging of the area at various altitude levels. Figure 2 shows 10 descent images taken from 1085 m to 8 m above the ground and covering an area of 1.5 km × 1.5 km. The images are approximately centered at a simulated landing point G1 in Figure 3a that describes the footprints of the six lower descent images in the overlapping area. Figure 3b illustrates the five additional images taken at approximately the same height in an extended area ∼1.5 km from the descending center. These five additional images cover a geologically interesting channel area and overlap with the descent images in Figure 2 also. The FIDO rover acquired data at three rover stations.

[21] Within the imaging area, 22 GCPs (ground control points) were surveyed using dGPS technology to assess the rover localization quality (Figure 4). The GCPs are distributed symmetrically around the descent center G1 and the alternative center G15. They were laid out as cross-shaped ground targets for identification in the descent images and surveyed using dGPS technology with an
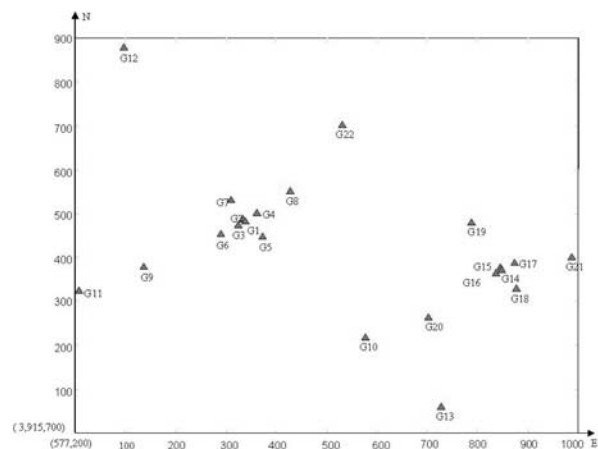
Figure 4. Distribution of ground control points.

Table 1. Standard Deviations of Exterior Orientation Parameters of the Descent Images

Photo-ID	Δ_X, m	Δ_Y, m	Δ_Z, m	Δ_ω, min:s	Δ_ϕ, min:s	Δ_κ, min:s	Altitude, m
P1	0.031	0.031	0.036	12:6.4	12:53.7	2:9.8	8
P2	0.058	0.054	0.035	10:28.7	11:13.0	1:42.7	18
P3	0.089	0.086	0.046	9:6.8	9:23.7	1:34.8	32
P4	0.112	0.095	0.053	5:50.8	6:56.0	1:19.3	55
P5	0.214	0.169	0.080	4:30.3	5:50.0	0:58.9	127
P6	0.241	0.194	0.087	4:32.7	5:47.4	1:2.5	143
P7	0.355	0.285	0.116	4:7.7	5:26.3	0:53.4	227
P8	0.356	0.270	0.141	4:14.9	5:29.8	1:1.2	219
P9	0.390	0.506	0.175	2:53.1	2:15.5	0:49.0	589
P10	0.774	0.660	0.336	2:6.6	2:21.6	0:47.3	1085

accuracy of 2–5 cm in a global reference system. A local coordinate system was constructed with the descending center G1 as the origin. In order to formulate the three constraints of scale, azimuth, and zenith, point G20 was supplied as a landmark relative to G1. Nine GCPs (G2, G3, G4, G5, G6, G7, G8, G9, and G12) that are covered by at least two consecutive descent images were selected as checkpoints.

[22] The FIDO stereo camera Navcam is mounted on the rover mast. It has a short baseline of ~25 cm and a wider FOV of 22.5°. The focal length of Navcam is 4.85 mm, and the valid frame size is 512 pixels × 486 pixels. The rover took images at three stations that are 5 m, 500 m, and 1.5 km from the descending center.

### 5.2. Processing of Descent Images

[23] Radial lens distortions are the dominant distortion source in the descent images (up to 10 pixels). Suppose r is the radial distance from the principal point to an image point ($r^2 = x^2 + y^2$) and k_1, k_2, k_3, and $k_4\delta$ are coefficients of the radial lens distortion model, the radial lens distortion correction can be expressed as $r = k_1 r + k_2 r^3 + k_3 r^5 + k_4 r^7$. The secondary decentering distortion that has the direction perpendicular to the radial distortion and is also called tangential distortion can be corrected in x and y directions: $dx = p_1 (r^2 + 2xy) + 2p_2xy$ and $dy = p_2 (r^2 + 2y^2) + 2p_1xy$, with p_1 and p_2 being coefficients of the decentering distortion. If a descent image is taken at an altitude of h on Mars, the correction for the Martian ground curvature, r_c, with the Martian radius R (3397 km equatorial radius and 3375 polar radius), is depicted as $\delta r_c = \frac{h_r^3}{2Rf'^2}$, where f is the focal length. Approximate positions of the camera exposure centers were estimated from the topographic maps and on-board GPS data. In a Mars descending process, an altimeter will provide the approximate heights of the images, while matching of landmarks that are in the descent images and previous images or maps leads to approximate horizontal positions. These landmarks may also be contained in the Mars Global Control Network. As long as the adjacent descent images have an overlapping rate, preferably greater than 30%, the approximate image orientation angles can be computed from the same landmarks. In this case, the images were taken almost vertically. We assumed that the initial values of the orientation angles ϕ and ω are 0 and the azimuth angle κ was estimated from the matched landmarks in the map. In fact, the bundle adjustment method does not require a high accuracy of the approximate position and orientation parameters of the images.

[24] Seventy-two tie points that are hierarchically distributed in the vertical direction were manually selected and measured to form a bundle adjustment network. A bundle adjustment with the tie points, the 10 descent images, and all the GCPs as checkpoints was performed. The image measurement error is 0.5 pixel, assuming that the zoom function is applied when measuring the points. The image measurement errors are employed to compute the weight matrix of the observations in the bundle adjustment. Table 1 lists estimated standard deviations of the exterior orientation parameters of the descent images. The computational results show that the standard deviations of the positional parameters increase as the altitude increases. The standard deviations of the angular parameters have an opposite trend. In terms of accuracy the results are nearly the same as that of bundle adjustment with ground control points [*Li et al.*, 2000]. This demonstrates that the free network bundle adjustment on descent images with the applied constraints can achieve the same accuracy as that with ground control.

[25] Furthermore, we also analyzed the relationship between the errors of the ground points and their distances from the descending center. The RMS errors calculated for nine checkpoints within 500 m from the descending center are 0.24, 0.15, and 0.38 m in the x, y, and z directions respectively. Figure 5 describes the regression result of this relationship. The curve shows, to some extent, the general trend that the farther away a point is, the lower its accuracy is. However, there is no linear relationship between the distance and the point accuracy. In fact, the point accuracy depends on a complex set of factors such as the geometric strength of the network, and the number and distribution of GCPs and tie points, among others. It is clear that elevation (z direction) has apparently lower accuracy, as expected, than the planimetric (x and y) directions.

[26] The above descent images and the computed orientation parameters were used to generate a digital terrain model (DTM) of the Silver Lake test area. First, the DTM was filled with an initial elevation computed from a few points, for example, tie points or GCPs. Second, a top-down scheme was used to register 10 pairs of adjacent descent images from higher images to lower images. Corresponding features between pairs were then matched through searching along epipolar lines using an area-based correlation followed by a least squares matching [*Ackermann*, 1984].
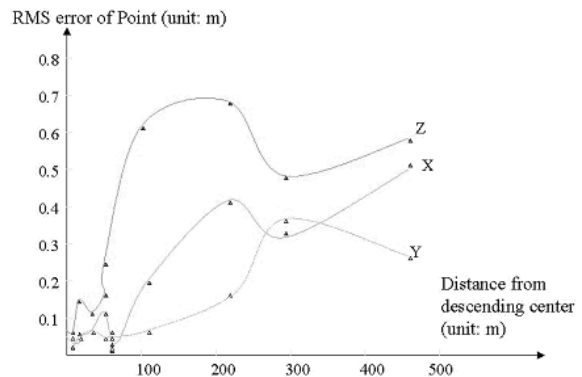
Figure 5. Ground point accuracy versus distance from the descending center (descent images only).
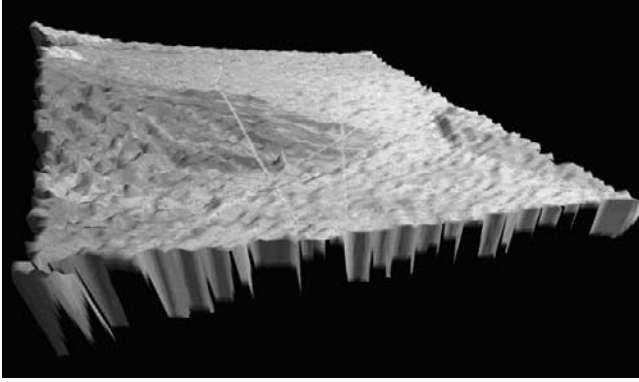
Figure 6. Perspective view of the digital terrain model (DTM) of the Silver Lake test field draped with a descent image.

Third, an initial DTM was built based on the matched features. Finally, a bottom-up scheme was applied to refine the DTM in which each grid point of the DTM was back-projected onto all possible overlapping descent images to find the corresponding features. A multiimage photogrammetric triangulation provided an improved elevation of the grid point. This process was applied to all the grid points to generate the final refined DTM displayed in Figure 6.

5.3. Rover Localization Using Descent and Rover Images

[27] An experiment for testing rover localization using descent and rover image data was performed with 11 descent images and 14 pairs of rover stereo images taken at stations that are 5 m, 500 m, and 1.5 km away from the descending center. Among them, four additional descent images are in the channel area that is ~1.5 km away from the descending center. In order to build a bundle adjustment network with both descent and rover image data, image features appearing in both kinds of images were selected as tie points (Figure 7).
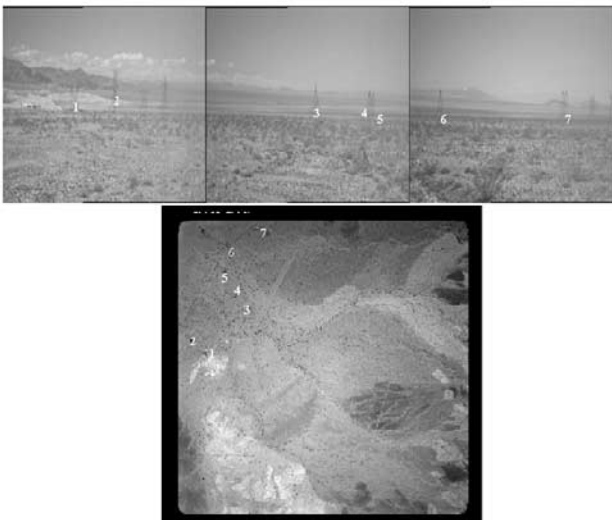
Table 2. Standard Deviations of Exterior Orientation Parameters for the Six Rover Images

Photo-ID	Δ_X, m	Δ_Y, m	Δ_Z, m	Δ_ω, min:s	Δ_ϕ, min:s	Δ_κ, min:s	Distance to Descent Center, m
1356	0.051	0.031	0.038	25:49.3	74:14.6	59:43.3	4.5
1404	0.050	0.032	0.036	24:36.1	73:22.7	57:34.8	4.5
4540	0.316	0.390	0.248	41:7.2	154:19.0	33:37.0	566.0
4611	0.328	0.386	0.253	41:41.4	154:53.0	34:36.0	566.0
1607	0.664	0.533	0.976	17:3.4	113:17.5	16:51.6	1518.3
1617	0.662	0.530	0.978	16:59.2	113:14.3	16:49.9	1518.3

[28] Table 2 lists the computed standard deviations of exterior orientation parameters of rover images that were taken at the three rover stations. The adjustment result shows that the positions of the rover cameras can be localized with an accuracy of 1 m within a distance of ~1.5 km from the descending center. The computed RMS errors of the ground coordinates of the checkpoints are 0.229, 0.205, and 0.455 m in the x, y, and y directions, respectively. Figure 8 demonstrates the relationship between the point accuracy and the distance from the descending center.

6. Conclusions

[29] Large-scale mapping of and rover localization on the Martian surface using descent and rover stereo images has been studied through the processing of the field data collected at the Silver Lake test site. On the basis of the above computational results and analysis, the RMS errors of coordinates in the x, y, and z directions are around 0.24, 0.15, and 0.38 m, respectively, for ground points within 500 m from the descending center. They are around 0.23, 0.21, and 0.46 m for ground points within 1.5 km from the descending center. The rover can be localized at an accuracy of about 1m over a distance of 1.5 km. Particularly, we draw the following conclusions:

Figure 7. Corresponding features between a (bottom) descent image and (top) rover images.
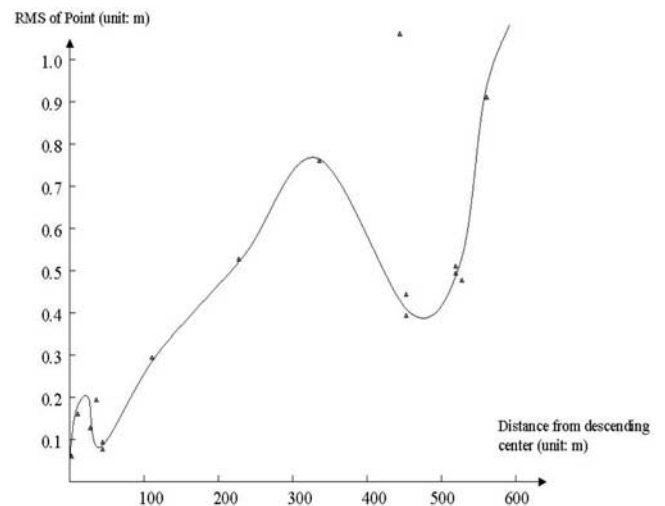
Figure 8. Ground point accuracy versus distance from the descending center (descent and rover images).

1. Rover localization through a bundle adjustment using descent and rover stereo images has the potential to achieve a rover localization accuracy of 0.1% of the distance traveled for Mars exploration. The combination of descent and rover image data offers the best way of localization for rover missions, including lowering mission risk by maximizing the ability to traverse to locations defined in a local frame, and also in the global frame if the local frame can be linked to it.

2. The result of the free network bundle adjustment demonstrated geometric and accuracy patterns similar to the bundle adjustment with ground control. This ensures that the developed computational model will fit the Mars landing site environment where no ground control will be available.

3. Rover locations in the boundary area of the descent image coverage can also be determined accurately if ground features or landmarks between the rover images and higher-altitude descent images can be recognized and precisely measured.

4. One of the keys in successful processing the descent and rover image data is to select a sufficient number of tie points that are evenly distributed in the imaged area. This is even more crucial to the free network bundle adjustment.

Notation

m element of rotation matrix.

k rotation angle about the z axis.

X_0 X coordinate of the exposure center in the (X, Y, Z) coordinate system.

Y_0 Y coordinate of the exposure center in the (X, Y, Z) coordinate system.

Z_0 Z coordinate of the exposure center in the (X, Y, Z) coordinate system.

X_p X coordinate of the object point in the (X, Y, Z) coordinate system.

Y_p Y coordinate of the object point in the (X, Y, Z) coordinate system.

Z_p Z coordinate of the object point in the (X, Y, Z) coordinate system.

f sensor focal length.

x x coordinate in the image coordinate system.

y y coordinate in the image coordinate system.

S distance between two ground points.

α azimuth angle.

β zenith angle.

L observation vector.

V correction vector.

X unknown vector.

A coefficient matrix of the observation equation.

H coefficient matrix of the constraint equation.

W residual vector.

N normal matrix of the observation equation.

σ_o^2 unit weight variance.

Σ_x co-variance matrix of X.

k_1, k_2, k_3, k_4 coefficients of the radial lens distortion.

δr correction of the radial lens distortion.

p_1, p_2 coefficients of the decentering distortion.

Dx, dy corrections of the decentering distortion.

δr_c correction for the Martian ground curvature.

h altitude of a descent image from the Martian surface.

R radius of Mars.

References

Ackermann, F., High precision digital image correlation, in *Schriftenreihe Institut fuer Photogrammetrie*, Univ. Stuttgart, Stuttgart, Germany, 1984.

Albertz, J., H. Ebener, and G. Neukum, The HRSC/WAOSS Camera Experiment on the Mars96 Mission-A photogrammetric and cartographic view of the project, *Int. Arch. Photogramm. Remote Sens., XXXI*, Part B4, 58–63, 1996.

Arvidson, R. E., S. W. Squyres, E. T. Baumgartner, P. S. Schenker, C. S. Niebur, K. W. Larsen, F. P. Seelos, N. O. Snider, and B. L. Jolliff, FIDO prototype Mars rover field trials, Black Rock Summit, Nevada, as test of the ability of robotic mobility systems to conduct field science, *J. Geophys. Res., 107*, 10.1029/2000JE001464, 2002.

Golombek, M. P., et al., Overview of the Mars Pathfinder Mission and assessment of landing site predictions, *Science, 278*, 1743–1748, 1997.

Li, R., F. Ma, F. Xu, L. Matthies, C. Olson, and Y. Xiong, Mars Rover localization using descent and rover imagery-result of the field test at Silver Lake, CA, in *Proceedings of ASPRS Annual Conference 2000* [CD-ROM], Washington, D.C., 2000.

Olson, C., and L. Matthies, Maximum likelihood rover localization by matching range maps, paper presented at IEEE International Conference on Robotics and Automation, Inst. of Electr. and Electron. Eng., Leuven, Belgium, 16–20 May 1998.

Pischel, R., D. de Niem, H. Hoffmann, and V. Mertens, HRSC Operations, paper presented at HRSC Science Team Meeting, Berlin, Germany, 9–11 May 2001.

Raeburn, P., and M. Golombek, *Uncovering the Secrets of the Red Planet: Mars*, 231 pp., Natl. Geogr. Soc., Washington, D.C., 1998.

Volpe, R., T. Litwin, and L. H. Matthies, Mobile robot localization by remote viewing of a colored cylinder, paper presented at International Conference on Robots and Systems (IROS), Inst. of Electr. and Electron. Eng., Pittsburgh, Pa., 5–9 Aug. 1995.

Wolf, P., *Elements of Photogrammetry*, 628 pp., McGraw-Hill, New York, 1983.

Zeitler, W., T. Ohlhof, and H. Ebner, Recomputation of the Global Mars Control Point Network, *Photogramm. Eng. Remote Sens., 66*(2), 155–161, 2000.

R. E. Arvidson, Department of Earth and Planetary Sciences, Washington University, St. Louis, MO 63130, USA.

R. Li, F. Ma, and F. Xu, Department of Civil and Environmental Engineering and Geodetic Science, Ohio State University, Columbus, OH 43210-1275, USA. (li.282@osu.edu)

L. H. Matthies and C. F. Olson, Jet Propulsion Laboratory, California Institute of Technology, Pasadena, CA 91125, USA.